Supporting information

Catalyst Support Effect on the Activity and Durability of Magnetic Nanoparticles: toward Design of Advanced Electrocatalyst for Full Water Splitting

Fatemeh Davodi [1], Elisabeth Mühlhausen [2], Mohammad Tavakkoli [1], Jani Sainio [3], Hua Jiang [3], Bilal Gökce [2], Galina Marzun [2], Tanja Kallio *[1]

[1] F. Davodi, Dr. M. Tavakkoli, Prof. T. Kallio

Electrochemical Energy Conversion Group, Department of Chemistry and Materials Science, School of Chemical Engineering, Aalto University, P.O. Box 16100, FI-00076 Aalto, Finland.
Email: tanja.kallio@aalto.fi

[2] E. Mühlhausen, Dr. G. Marzun, Dr. B. Gökce
University of Duisburg-Essen, Technical Chemistry I and Center for Nanointegration Duisburg-Essen (CENIDE), Universitätsstr. 7, 45141 Essen, Germany

[3] Dr. J. Sainio, Dr. H. Jiang
Department of Applied Physics, School of Science, Aalto University, P.O. Box 15100, FI 00076 Aalto, Finland.

Calculation of electrochemically active surface area

The electrochemical capacitance was calculated by measuring double layer capacitance of Ni@γ-Fe_2O_3/ES-MWNT on a glassy carbon RDE in 1 M NaOH as descried earlier. [3] To measure the double layer capacitance, the cyclic voltammograms (CVs) were plottet at different scan rates in a potential range where no Faradaic process occurred (Fig. S7a) and charging currents (i_c) at different scan rates were measured. From the slope of i_c as a function of scan rate (v), the double layer capacitance (C_{DL}) was obtained (Fig. S7b) based on the following eq. 1:

$$i_c = vC_{DL} \quad (1)$$

The C_{DL} of Ni@γ-Fe_2O_3/ES-MWNT measured by the above-mentioned method is ~ 1.38 mF. The electrochemically active surface area (ECAS) can be obtained from eq 2:

$$\text{ECAS} = C_{DL}/C_s \quad (2)$$

Where C_s is the specific capacitance. The average C_s of 0.040 mF cm^{-2} in 0.1 M NaOH was used for the calculation of the ECAS based on previous reports[3] in alkaline solution. As a result, an ECAS of 35 cm^2 was obtained for the Ni@γ-Fe_2O_3/ES-MWNT catalyst.

Estimation of the Faradaic efficiency

The experiments were performed in a rotating ring-disk electrode (RRDE) configuration. The Pt-ring electrode was set at 0.4 V vs. RHE to allow the O_2 produced on the disk during the anodic scans to be reduced, via 4 electrons, to OH^-, according to equation (3):

$$O_2 + 2H_2O + 4e^- \rightarrow 4OH^- \qquad (3)$$

The faradaic efficiency (ε%) was calculated using the expression for the collection efficiency of the RRDE given in eq 4:

$$\varepsilon\% = \frac{j_{ring}}{N * j_{disk}} * 100 \qquad (4)$$

Where j_{ORR} and j_{OER} are current densities measured on the Pt ring and the GC disk, respectively, and N is the collection efficiency (here ~0.2) of the RRDE.

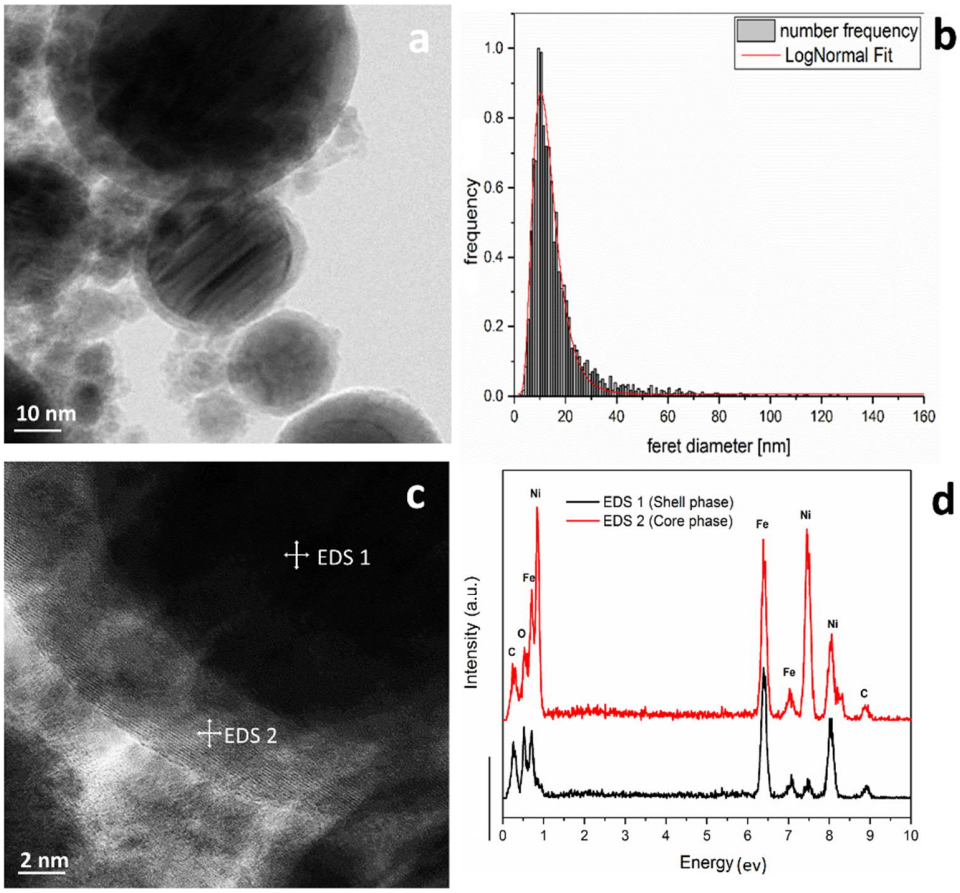

Figure S1. (a) TEM images obtained from the Ni@γ-Fe_2O_3 nanoparticles, (b) Particle size distribution of the Ni@γ-Fe_2O_3 nanoparticles received from the TEM images. The average diameter obtained from the LogNormal fit is 12.3 nm, (c) HR-TEM image of an isolated Ni@γ-Fe_2O_3 particle showing the interface of the core (Ni) and shell (γ-Fe_2O_3) in the particle, and (d) corresponding EDS spectra from the particle, showing elemental compositions of the shell and the core.

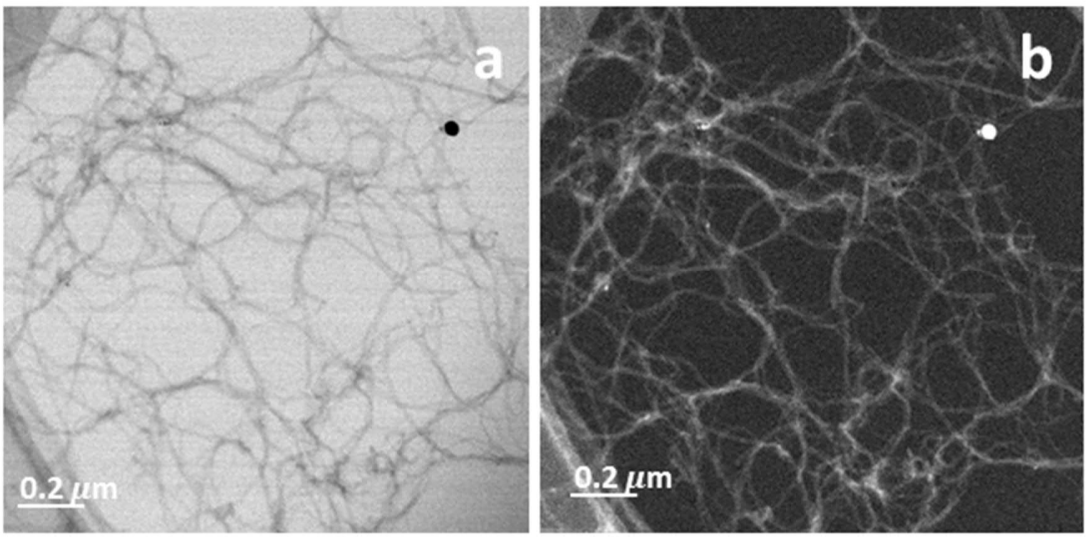

Figure S2. (a) STEM and corresponding (b) HAAD-STEM images obtained from MWNTs (without ES functionalization) mixed with the Ni@γ-Fe_2O_3 particles, showing very sparse dispersion of the particles on MWNTs in the absence of the ES polymer.

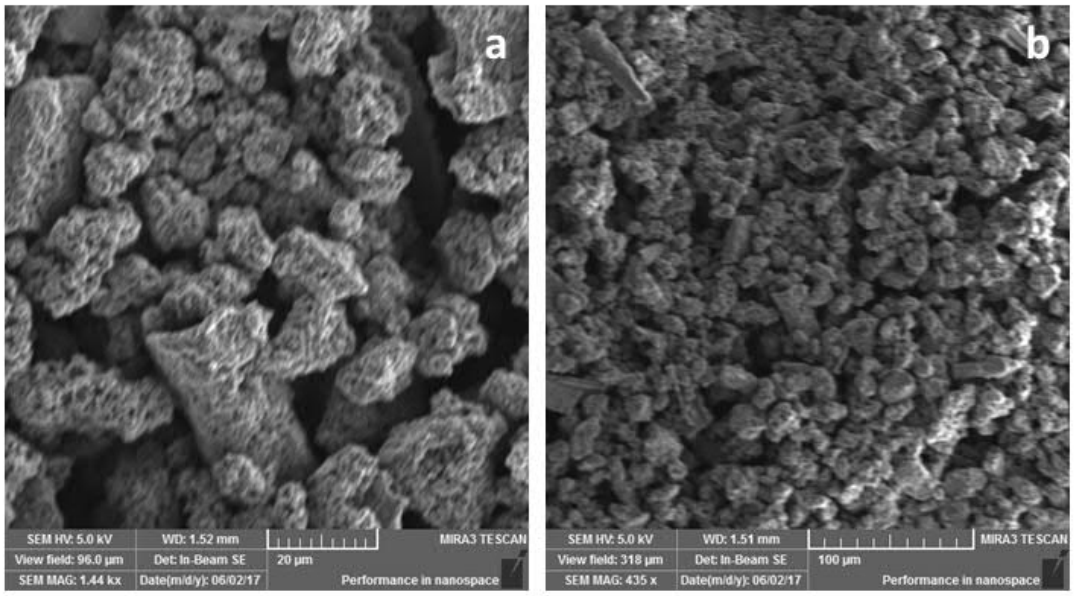

Figure S3. (a) A high-resolution and (b) low resolution scanning electron microscopy images of the Ni@γ-Fe_2O_3 nanoparticles mixed with emeraldine salt polymer.

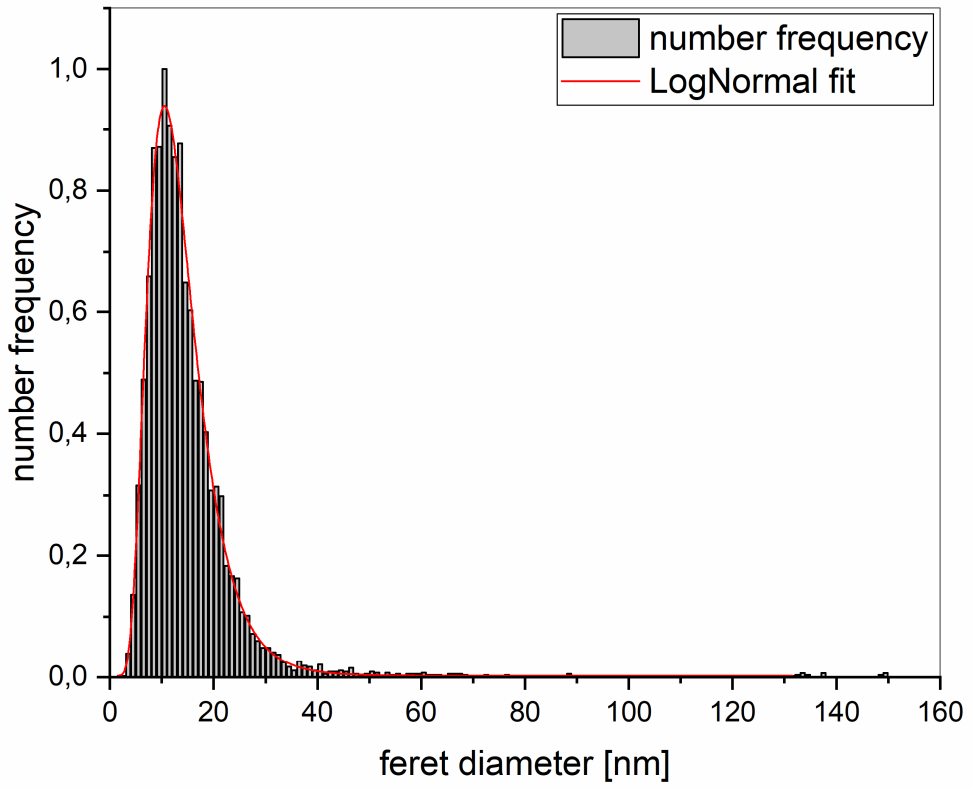

Figure S4. Particle size distribution of the FeO_x nanoparticles received from the TEM images. The average diameter obtained from the LogNormal fit is 12.5 nm.

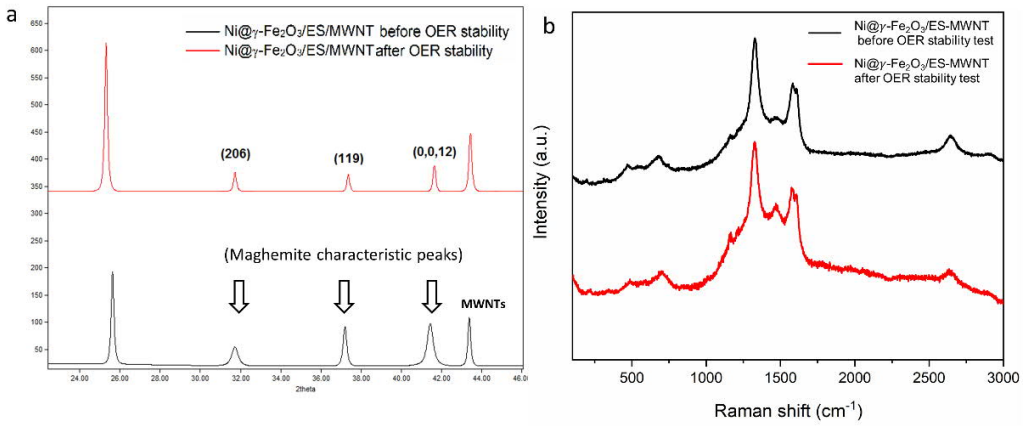

Figure S5. (a) XRD and (b) Raman spectra of Ni@γ-Fe_2O_3/ES-MWNT before (black line) and after (red line) of the 5,000 OER cycles.

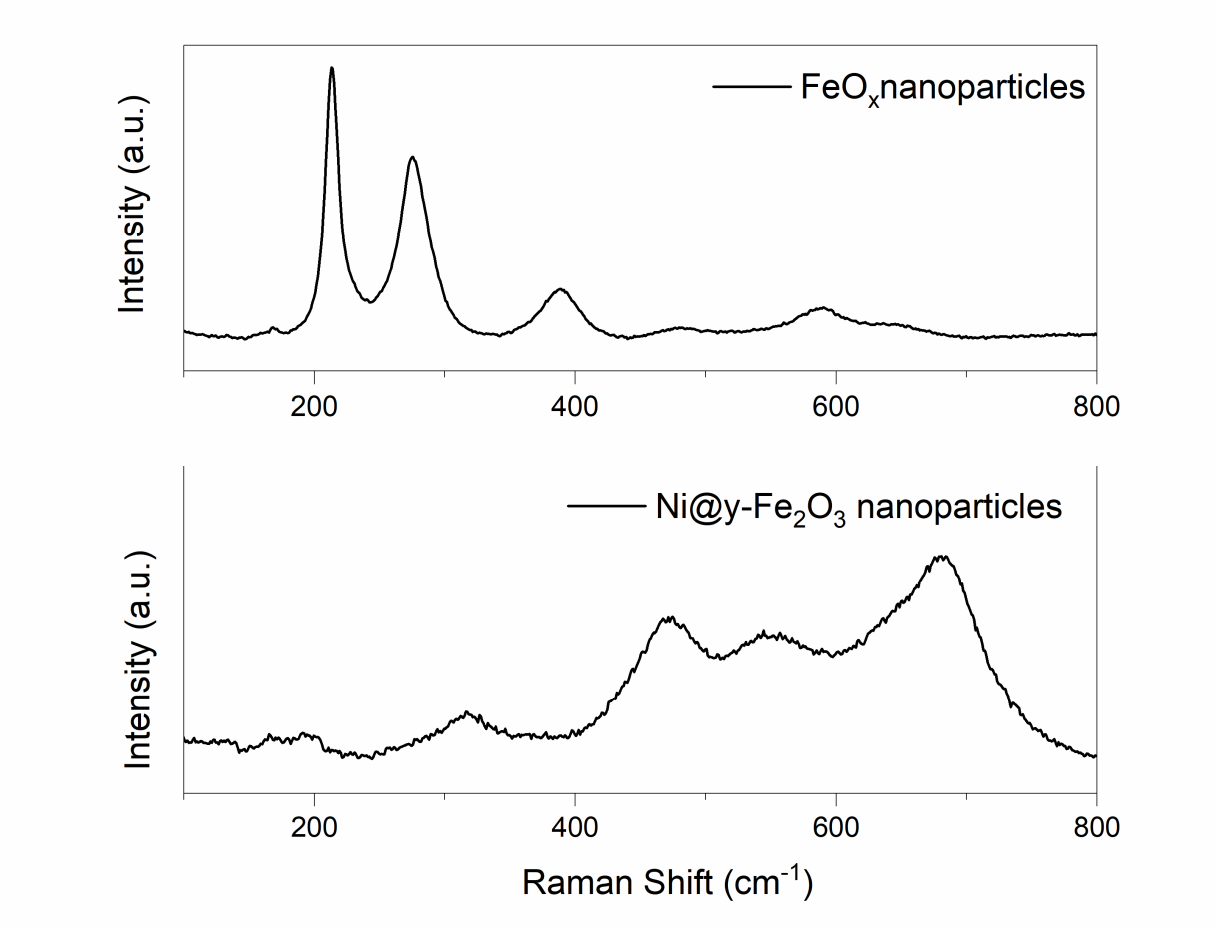

Figure S6. Raman spectra of FeO_x NPs (above) and Ni@γ-Fe_2O_3 NPs (below), showing hematite and maghemite Raman features, respectively.

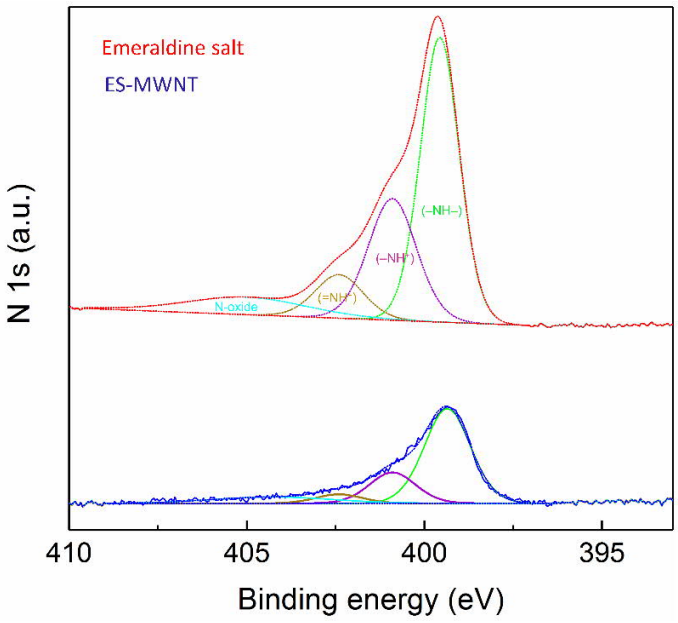

Figure S7. X-ray photoelectron spectra of N 1s obtained from emeraldine salt and MWNT-ES. Deconvoluted components shown: amine (green line), protonated amine (purple line), protonated imine (yellow line) and N-oxide (light blue line).

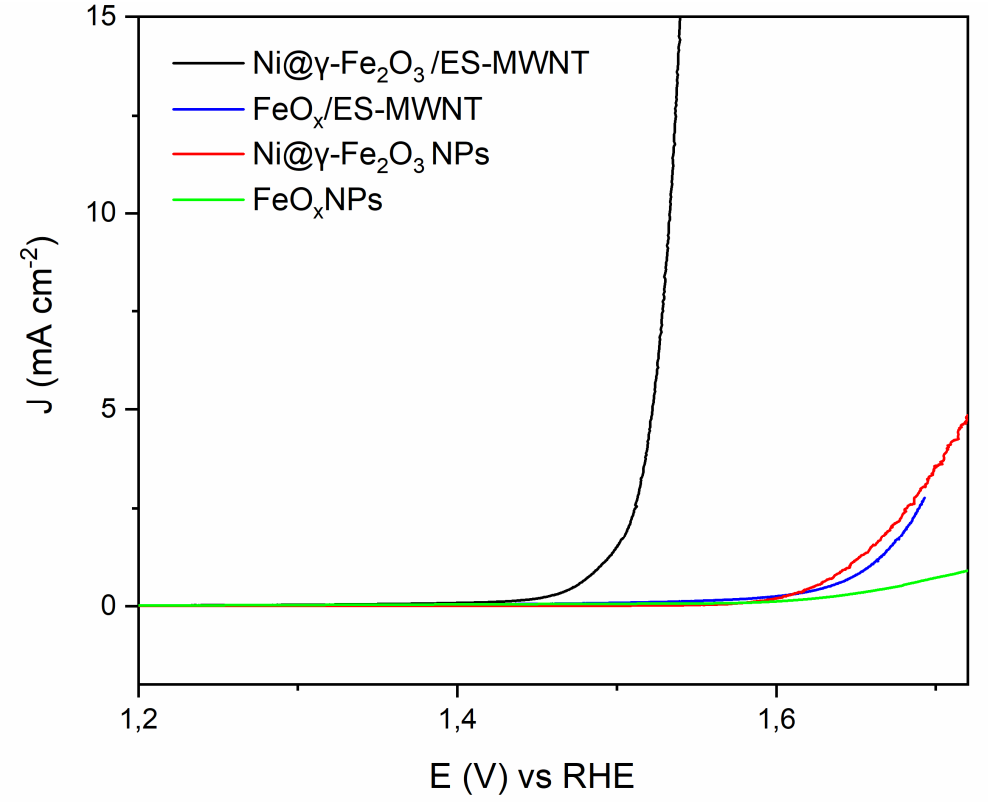

Figure S8. IR-corrected RDE polarization curves obtained with the FeO_x NPs (green line), Ni@γ-Fe_2O_3 NPs (red line), FeO_x/ES-MWNT (blue line) and Ni@γ-Fe_2O_3/ES-MWNT (black line) in 0.1 M NaOH solution. The curves were measured at a scan rate of 5 mV s^{-1} and a rotation speed of 1600 rpm.

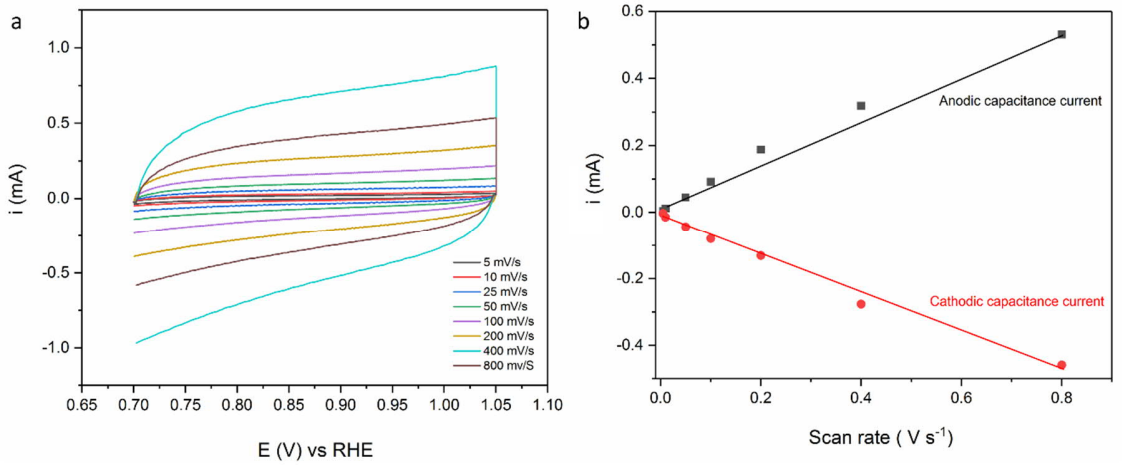

Figure S9. Double-layer capacitance measurements for the Ni@γ-Fe_2O_3/ES-MWNT catalyst from cyclic voltammetry in 1 M NaOH. (**a**) Cyclic voltammograms of the N i@γ-Fe_2O_3/ES-MWNT electrode recorded in a non-faradaic region (0.7 - 1.05 V vs. RHE) at scan rates of 5, 10, 25, 50, 100, 200, 400, and 800 mV. The working electrode was held at each potential for 20 s before beginning of the next sweep. Current in this graph was assumed to be induced only by capacitive charging/discharging. (**b**) The cathodic (red circle) and anodic (black square) capacitance currents measured at 0.95 V vs. RHE are plotted as a function of the scan rate. The double-layer capacitance of this system is calculated as the average of the absolute value of the slope of the linear fits to the data (see the equations above).

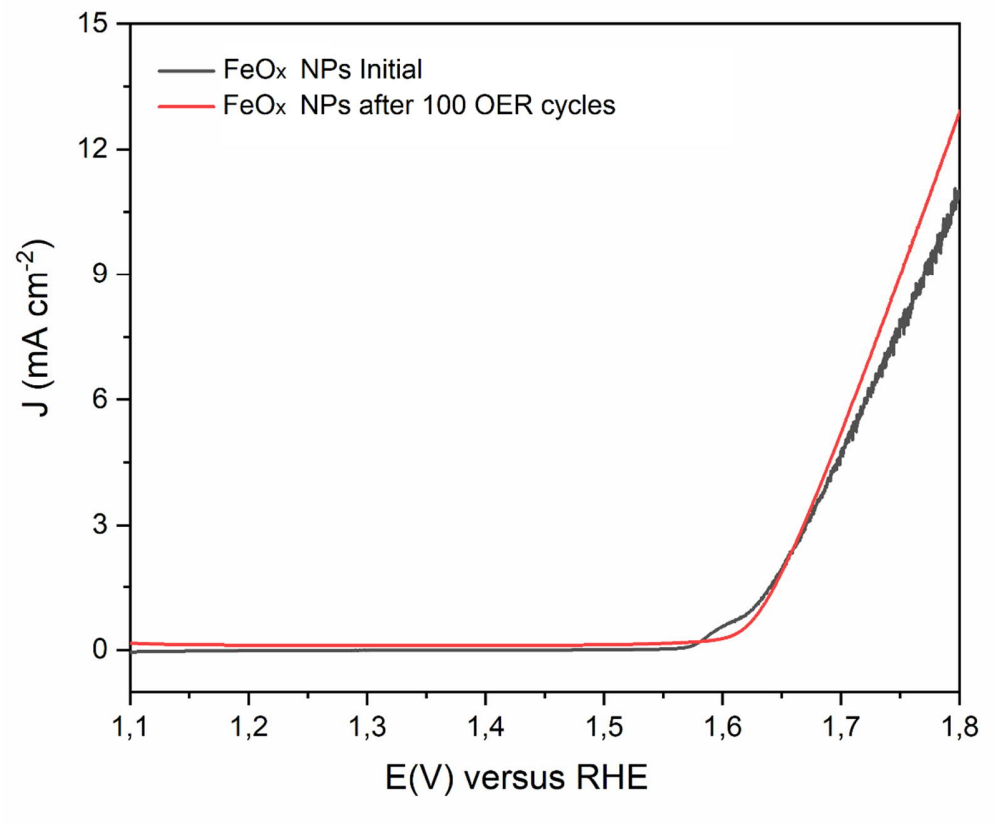

Figure S10. OER polarization curves of the FeO_x NPs before (red solid line) and after (black line) 100 stability cycles between 1 and 1.75 V vs RHE at a scan rate of 50 mV s^{-1} in 0.1 NaOH,

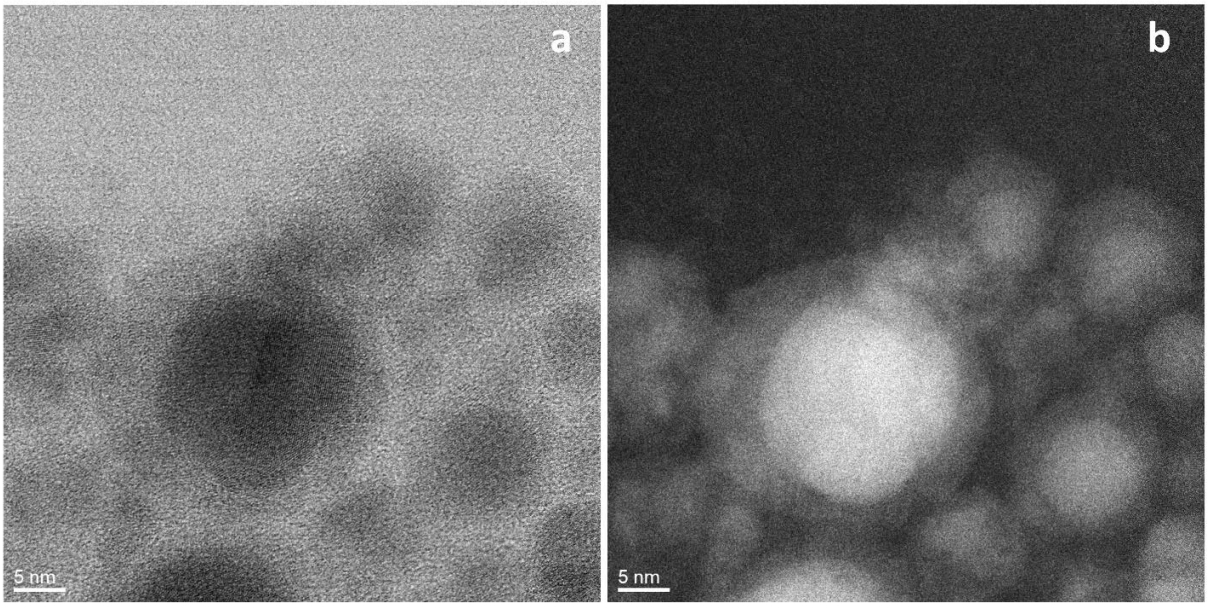

Figure S11. Structural and elemental analysis of Ni@γ-Fe_2O_3 after electrochemical stability measurements. (a) STEM and corresponding (b) HAAD-STEM images of the Ni@γ-Fe_2O_3 core-shell NPs.

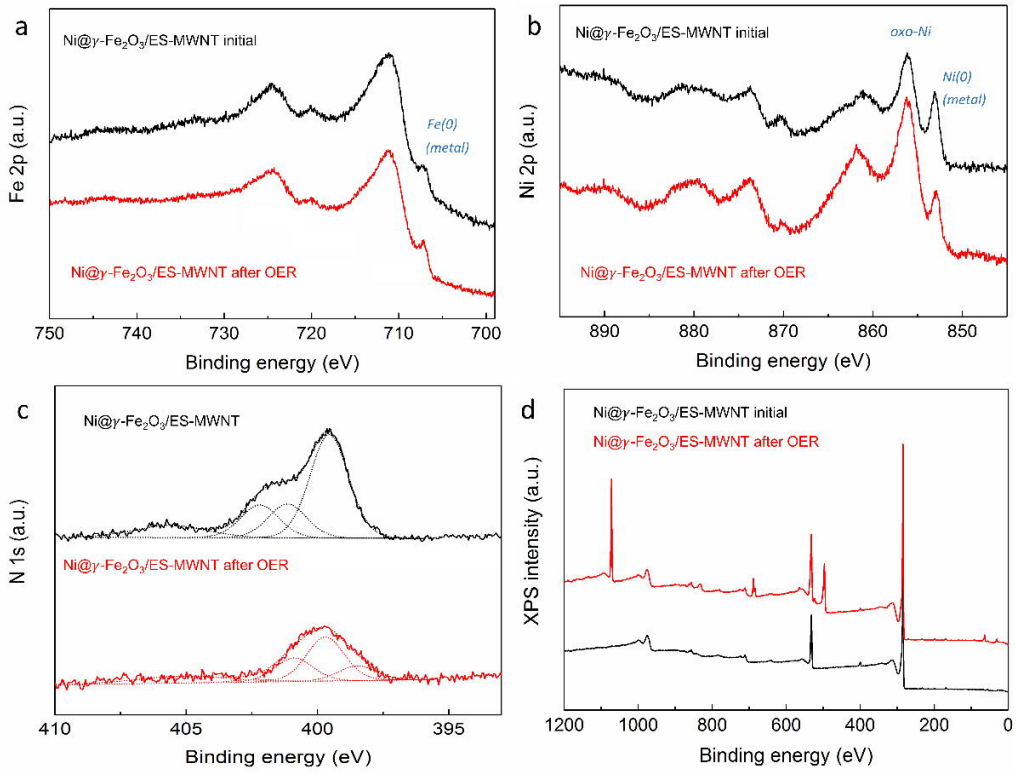

Figure S12. (a) Fe 2p, (b) Ni 2p, (c) N 1s and (d) survey XPS spectra of the Ni@γ-Fe_2O_3/ES-MWNT catalyst before and after the 5,000 OER cycles.

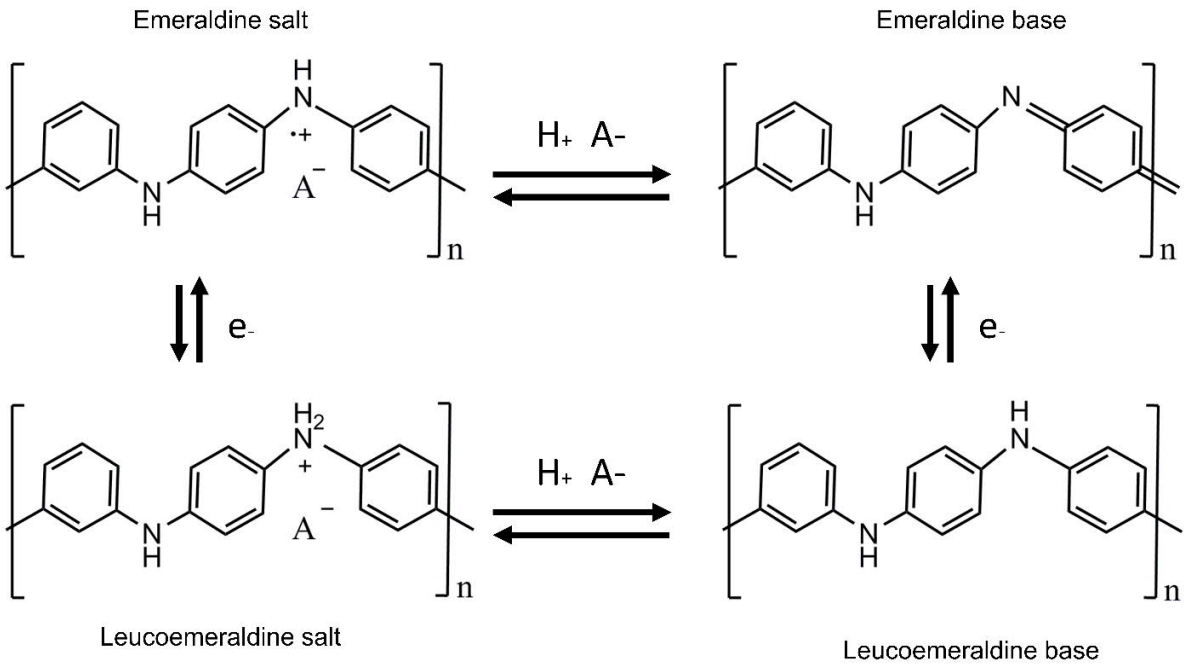

Figure S13. Different chemical structures of polyaniline emeraldine salt.

Table S1 The atomic percentages of the different elements of Ni@γ-Fe_2O_3/ES-MWNT (before and after the stability measurements), emeraldine salt (ES), and the ES-MWNT composite as derived from XPS. The error bar associated with atomic percentage is of the order of ±10% of the value. Note that for the Ni@γ-Fe_2O_3/ES-MWNT sample tested for the OER, Nafion was used as binder. Therefore, the presence of Nafion on the Ni@γ-Fe_2O_3/ES-MWNT after the OER can underestimate the real N/C ratio.

Catalyst	Ni (at-%)	Fe (at-%)	N (at-%)	C (at-%)	S (at-%)	F (at-%)	O (at-%)	Na (at-%)	Cl (at-%)
Emeraldine salt	-	-	7.28	79.7	2.72	0.49	9.80	-	-
ES-MWNT	-	-	1.42	94.7	0.46	0.14	3.20	0.03	0.05
Ni@γ-Fe_2O_3/ ES-MWNT	0.40	0.54	1.54	84.2	0.36	0.05	12.8	0.04	0.04
Ni@γ-Fe_2O_3/ ES-MWNT after stability measurments	0.48	0.42	0.48	75.6	0.25	3.54	14.4	4.72	0.14

Table S2 The percentages of different nitrogen species of all nitrogen for Ni@γ-Fe_2O_3/ES/MWNT (before and after the OER stability measurements), ES, and ES-MWNT composite as derived from peak fitting of the N 1s XPS region (BE = binding energy).

catalyst	imine (=N-) BE~398.5 eV	amine (-NH-) BE~399.5 eV	protonated amine ($-NH_2^+$) BE~401.1 eV	protonated imine ($=NH^+$) BE~402.2 eV	N-oxide BE~404-406 eV
Emeraldine salt	-	52	28	10	10
ES-MWNT	-	62	21	6	11
Ni@γ-Fe_2O_3/ES-MWNT	-	54	17	17	12
Ni@γ-Fe_2O_3/ES-MWNT after measurments	15	43	23	3	16

Table S3 Comparison of OER performance of the Ni@γ-Fe_2O_3/ES-MWNT catalyst to the state-of the-art OER material, so far reported γ-Fe_2O_3 containing electrocatalyst and core-shell metal@Fe_xO reported electrocatalyst.

Catalyst	Electrolyte	η onset (mV)	η (mV) @ 10 mA cm^{-2}	Tafel slope (mV dec^{-1})	Mass loading (mg cm^{-2})	Substrate	Reference
Ni@γ-Fe_2O_3/ES-MWNT	0.1 M NaOH	250	290	45	0.2	GC	This work
	1 M NaOH	200	260				
γ-Fe_2O_3/CNT	0.1 M NaOH	340	410	50	0.2	GC	[3] 2016
	1 M NaOH	320	560				
γ-Fe_2O_3@NCNT	0.1M KOH	370	450	53	N.A	CP	[4] 2016
NiFe-LDH	0.1M KOH	280	300	35	0.25	GC	[5] 2013
state-of-the-art	1M KOH	220	240				
Au@$CoFeO_x$	1M KOH	260	350	N.A	N.A	GC	[6] 2017
Ni-bipy-MWCNT	0.1 M NaOH	290	310	35	0.2	GC	[7] 2017
	1 M NaOH	260	290				

References:

1 S. Barcikowski, T. Baranowski, Y. Durmus, U. Wiedwald and B. Gökce, *J. Mater. Chem. C*, 2015, **3**, 10699–10704.

2 X. Yan, Z. Han, Y. Yang and B. Tay, *J. Phys. Chem. C*, 2007, **3**, 4125–4131.

3 M. Tavakkoli, T. Kallio, O. Reynaud, A. G. Nasibulin, J. Sainio, H. Jiang, E. I. Kauppinen and K. Laasonen, *J. Mater. Chem. A Mater. energy Sustain.*, 2016, **4**, 5216–5222.

4 T. Sharifi, W. L. Kwong, H. M. Berends, C. Larsen, J. Messinger and T. Wågberg, *Int. J. Hydrogen Energy*, 2016, **41**, 69–78.

5 M. Gong, Y. Li, H. Wang, Y. Liang, J. Z. Wu, J. Zhou, J. Wang, T. Regier, F. Wei and H. Dai, *J. Am. Chem. Soc.*, 2013, **135**, 8452–8455.

6 A. L. Strickler, M. Escudero-Escribano and T. F. Jaramillo, *Nano Lett.*, 2017, **17**, 6040–6046.

7 M. Tavakkoli, M. Nosek, J. Sainio, F. Davodi, T. Kallio, P. M. Joensuu and K. E. Laasonen, *ACS Catal.*, 2017, **7**, 8033−8041.